Proc. Natl. Acad. Sci. USA
Vol. 93, pp. 3330–3334, April 1996
Biochemistry

Crystal structure of the T state of allosteric yeast chorismate mutase and comparison with the R state

(allosteric enzyme/enzyme regulation/x-ray diffraction/heterotropic effector/conformational change)

NORBERT STRÄTER*, KJELL HÅKANSSON*†, GEORG SCHNAPPAUF‡, GERHARD BRAUS‡, AND WILLIAM N. LIPSCOMB*§

*Gibbs Chemical Laboratory, Harvard University, 12 Oxford Street, Cambridge, MA 02138; and ‡Institut für Mikrobiologie, Biochemie und Genetik, Friedrich-Alexander-Universität, Staudtstrasse 5, D-91058 Erlangen, Germany

Contributed by William N. Lipscomb, December 22, 1995

ABSTRACT **The crystal structure of the tyrosine-bound T state of allosteric yeast *Saccharomyces cerevisiae* chorismate mutase was solved by molecular replacement at a resolution of 2.8 Å using a monomer of the R-state structure as the search model. The allosteric inhibitor tyrosine was found to bind in the T state at the same binding site as the allosteric activator tryptophan binds in the R state, thus defining one regulatory binding site for each monomer. Activation by tryptophan is caused by the larger steric size of its side chain, thereby pushing apart the allosteric domain of one monomer and helix H8 of the catalytic domain of the other monomer. Inhibition is caused by polar contacts of tyrosine with Arg-75 and Arg-76 of one monomer and with Gly-141, Ser-142, and Thr-145 of the other monomer, thereby bringing the allosteric and catalytic domains closer together. The allosteric transition includes an 8° rotation of each of the two catalytic domains relative to the allosteric domains of each monomer (domain closure). Alternatively, this transition can be described as a 15° rotation of the catalytic domains of the dimer relative to each other.**

Chorismic acid lies in the main branch point of the biosynthetic pathway of the aromatic amino acids tryptophan, phenylalanine, and tyrosine (1, 2). In one branch, which eventually leads to the production of tryptophan, chorismate is the substrate of the anthranilate synthase complex. In the other branch, chorismate mutase (chorismate pyruvatemutase, EC 5.4.99.5) catalyzes the intramolecular rearrangement of chorismate to prephenate, the first committed step in the synthesis of tyrosine and phenylalanine. Notably, this rearrangement reaction is the only known enzymatically catalyzed pericyclic process. The reaction probably proceeds via a chair-like transition state (3–6), which is stabilized in an energetically favorable environment of the enzyme active site (Fig. 1). This stabilization can be achieved without the involvement of any functional group, as implicated from kinetic and structural studies on *Bacillus subtilis* chorismate mutase (7, 8). However, the structures of the chorismate mutases (CM) from yeast *Saccharomyces cerevisiae* (YCM; ref. 9) and from the P protein from *Escherichia coli* (10, 11) have been compared, revealing the active site side chains for YCM (12), including the presumably protonated carboxylate group of Glu-246 (Gln-88 in *E. coli* CM) interacting with the ether oxygen of the substrate. Thus, YCM may indeed have a functional catalytic residue.

YCM is a homodimer of two 30-kDa polypeptides. This enzyme is regulated by an allosteric mechanism in which tryptophan activates the wild-type enzyme ≈10-fold (K_a = 0.0015 mM) and tyrosine inhibits the enzyme by a factor of 10 (K_i = 0.05 mM) (13). Activation and inhibition are mainly achieved by a change in substrate affinity rather than by influencing k_{cat}. Whereas the R form has a pH optimum at 7.0, optimum activity is seen at pH 5.0 in the T form. The enzyme can be trapped in the R state by mutating Thr-226 to isoleucine (13). Although this mutant enzyme still binds tryptophan, it does not bind tyrosine. It was this T226I mutant for which the crystal structure of the R state could be solved at a resolution of 2.2 Å (9). Although no tryptophan was present in the crystallization buffer, two tryptophan molecules were located per dimer at the dimer interface.

YCM has essentially an all-helix structure, which has similarities (12) to the CM domain of the P protein from *E. coli*. Both proteins contain a four-helix bundle that surrounds the active site cavity. Using 94 residues of 22% sequence identity, these helix bundles can be superimposed with a root-mean-square deviation (rmsd) of 1.06 Å (12). However, unlike YCM, the *E. coli* enzyme is not allosterically regulated. As a relatively small protein in the allosteric family, YCM provides an ideal model system for exploring the detailed mechanisms of allosteric regulation as well as extending our knowledge of the catalytic mechanism. We describe here the crystal and molecular structures of the T form of wild-type YCM crystallized in the presence of tyrosine, and compare the T and R states to illuminate the allosteric mechanism.¶

MATERIALS AND METHODS

YCM was isolated as described (13). The protein was crystallized by the hanging-drop method by using 2.1 M ammonium sulfate, 55 mM sodium acetate (pH 5.0), 2 mM dithiothreitol, and 0.7 mM L-tyrosine as the reservoir solution. The drop contained a 1:1 mixture of 15 mg/ml YCM and the reservoir solution. Small crystals appeared overnight at 20°C. To grow the crystals to a size sufficient for x-ray diffraction, a single crystal was seeded once into a hanging drop of protein and crystallization buffer as described above, except that the drop has been preequilibrated overnight against a reservoir containing 1.8 M instead of 2.1 M ammonium sulfate. Using this procedure, tetragonal bipyramidal crystals of dimensions 0.2 × 0.2 × 0.2 mm can be obtained within 2 days. One crystal was prepared for cryo-cooling data collection by transferring the crystal stepwise for 30 min into reservoir solutions containing increasing concentrations of glycerol until a concentration of 30% (vol/vol) of the cryo-protectant was reached. X-ray diffraction data were collected at −150°C on a Siemens (Madison, WI) model X-1000 multiwire area detector. The crystal was mounted in a hair-loop free-standing film of the cryo-buffer. Table 1 summarizes the details of data collection and data reduction, which used, in part, the program XDS (14).

The publication costs of this article were defrayed in part by page charge payment. This article must therefore be hereby marked "*advertisement*" in accordance with 18 U.S.C. §1734 solely to indicate this fact.

Abbreviations: rmsd, root-mean-square deviation; tyr and trp, tyrosine and tryptophan at the allosteric binding site; YCM, yeast chorismate mutase; CM, chorismate mutase.

†Present address: Laboratory of Molecular Biophysics, Rex Richards Building, South Parks Road, Oxford OX1 3QU, United Kingdom.
§To whom reprint requests should be addressed.

¶The atomic coordinates have been deposited in the Protein Data Bank, Chemistry Department, Brookhaven National Laboratory, Upton, NY 11973 (file name 2CSM).

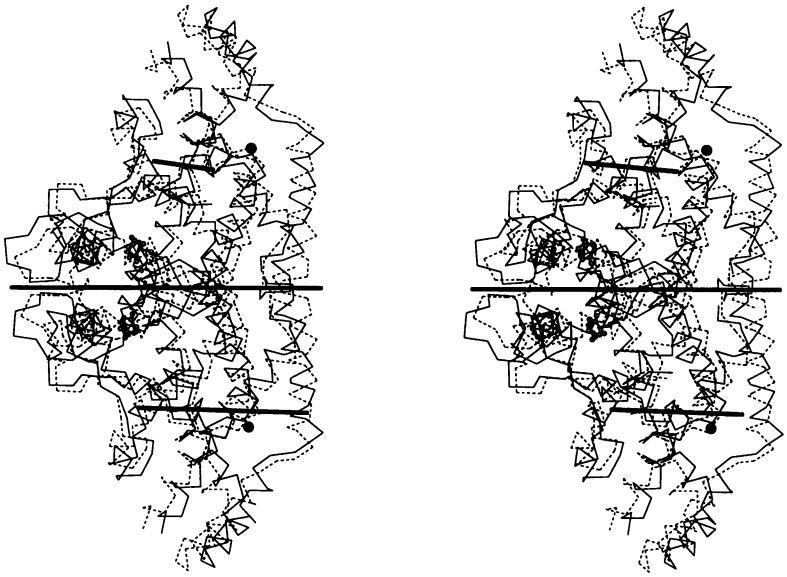

FIG. 1. Superposition of the dimer structures of yeast chorismate mutase (YCM) in the T state and R state (broken lines). Also shown are the two-fold dimer axis and the axes describing the allosteric transition and the model for noncovalently bound L-tyrosine. A point marks the center of the catalytic site.

Somewhat to our surprise, we were able to use the coordinates of the T226I mutant in its R state for solution of the structure of the T form by molecular replacement. The rotation and translation functions were solved with the program AMORE (15) using one monomer of the dimer, including the side chains as the search model. A promising peak of the translation function could be found only in the space group $P4_32_12$ and not in the enantiomorph $P4_12_12$. Placement of the monomer into the asymmetric unit resulted in a crystallographic R factor of 0.441 after rigid body minimization. Then, crystallographic refinement was performed using XPLOR (16). Ten percent of the measured reflections were set aside throughout all refinement steps and were used to calculate the free R factor (17). The model was refined by several rounds of manual rebuilding, simulated annealing (18), and positional minimization. All model building was done using the program O (19). The structural model for the noncovalently bound L-tyrosine (tyr) was included in the refinement only after most of the protein was already well refined, and when the difference electron density ($F_o - F_c$) for the inhibitor was well defined. This density, which even before it was introduced in the refinement had the shape of a tyrosine molecule, could not be interpreted as any protein side chain. Also, its refined temperature factors were reasonably low (Table 1). The density of the phenol ring of this tyrosine was not as flat as that of the well-defined tyrosine side chains of the protein, suggesting some disorder with respect to a nutational motion of the phenol group. Solvent molecules were added from the electron density in $|F_o - F_c|$ maps, provided they showed reasonable hydrogen bond geometry and contacts. Water molecules with temperature factors of more than 50 Å^2 after refinement were removed from the model. The electron density of the protein was generally well defined. An exception is the loop from residue 215 to 223 (220s loop), which was omitted from the model. Also, the loop from 47 to 55, which was included in the model, seems to be partially disordered; this region has weak or ill-defined density. In the previous study of the R state, the 220s loop also was omitted because of no density, and the 50s loop showed significantly higher-than-average temperature factors (9). The matrices for a superposition of different models or regions were calculated by a least-squares distance minimization algorithm implemented inside O using the C_α atoms as the guide coordinates, even if the rmsd difference was analyzed for other atom types. A Luzzati (20) analysis was used to estimate the coordinate error as 0.3–0.35 Å. Details of the refinement are listed in Table 1. All figures have been prepared using MOLSCRIPT (21).

Table 1. Details of data collection and refinement

	Factor
Data set statistics	
Space group	$P4_32_12$
Cell axes, Å	a = 78.6, c = 116.1
Maximum resolution, Å	2.8
No. of crystals	1
Temperature, °C	−150
Reflections, measured/unique	29418/9401
Completeness, %*	99.1 (97.3)
Completeness > $2\sigma_F$, %*	92.1 (76.1)
R_{svm}*	0.069 (0.28)
V_m, Å^3/Da	3.0
Refinement statistics	
Resolution range, Å*	7.0–2.8 (2.9–2.8)
R/R_{free}	0.213/0.321
Protein/water/ligand atoms ($Z > 1$)	2012/31/13
rmsd bond length, Å/angles, °	0.007/1.6
Dihedrals/impropers, °	19.4/1.3
B_{av} protein/waters/ligands, Å^2	22.4/26.6/21.4
Ramachandran plot outliers	0

*Values in parentheses are for the highest resolution shell.

RESULTS AND DISCUSSION

Monomer and Dimer Structure. A comparison of the structures of T and R state YCM shows that the secondary structure elements are largely the same in both states (Table 2). Differences are seen in the length of some elements and the short 3_{10}-helix H3 of the T form becomes an α-helix in the R form. However, significant movements and rearrangements occur within each monomer as well as of the two monomers relative to each other. To evaluate these differences, the C_α coordinates of the two structures were superimposed. When all C_α coordinates of the dimer were superimposed, the rmsd is 2.4 Å. If all C_α coordinates of one monomer are superimposed, the rmsd is 1.6 Å. The C_αs of the region of residues 1–45, 100–213,

Table 2. Superposition of secondary structure elements (SSE) between T and R states for monomers A and B

SSE	Residue	rmsd*			Note†
		Int.	A	B	
H1	6–9	0.1	0.6	5.7	
H2	14–33	0.6	1.4	4.2	dim, reg, act
L30s	34–39	0.2	1.3	3.6	
H3	40–43	0.1	0.8	4.0	
L50s	44–58	1.6	2.5	5.5	flexible
H4	59–73	0.3	2.9	4.4	dim
H5	76–78	0.0	3.1	4.6	reg
L80s	79–107	1.2	3.1	5.4	
H6	108–110	0.0	1.0	7.5	
H7	113–129	0.3	1.3	4.4	
L130s	130–139	0.3	1.0	3.5	reg
H8	140–171	0.4	0.8	5.3	dim, reg, act
H9	173–181	0.2	0.7	11.0	
H10	185–192	0.3	1.1	9.7	
H11	195–211	0.4	1.3	6.1	act
L220s	212–226				disorder
H12	227–251	1.2	1.6	7.0	act

*Int., rmsd when this secondary structural element is superimposed using only C_α atoms of this element, as a measure of its internal distortion in the T-to-R transition. The rmsds for monomer A and B were calculated after superposition of C_α atoms of the T and R structures of the regions 1–45, 56–214, and 224–254 of monomer A.
†act, Active site; reg, regulatory site; dim, dimer interface.

and 231–254, which superimpose with an rmsd of 1.1 Å, include the four-helix bundle and the active site region. This superposition excludes the 50s and 80s loops and helices H4 and H5, which move relative to the catalytic domain (Table 2, Fig. 1). The other monomer shows an rmsd of 6.1 Å after this superposition, which indicates a significant movement of the two monomers relative to each other in the T to R transition.

After superposition of the dimers of the two allosteric states, the transition from the T to the R state may be described as a rotation of each monomer by 8° around axes passing approximately through the center of the monomers as shown in Figs. 1 and 2. The two axes have angles of 77.2° and 112.4° with the dimer axis. The rotation is such that helix H8, which forms part of the dimer interface and the tyr/trp binding site (trp, tryptophan at the allosteric binding site; see below), moves away from the allosteric site.‖ The translational component is 0.7 Å along the rotation axes. However, the 80s loop and helices H4/H5 do not follow this rotation, but display a smaller shift of about 1.5 Å away from each allosteric site in a direction opposite from that implied by the rotation of the four-helix bundle, including the catalytic site. We can thus divide the structure of a YCM monomer into an allosteric domain comprising L50s, H4, L80s, and H5 and a catalytic domain containing the remaining structural elements, except for L220s, which might also play a special role in the allosteric transition. The C_α of trp moves by 2 Å relative to the C_α of tyr in the same direction as the movements of the nearby residues of helix H8.

The rotation of the two monomers relative to each other may alternatively be described as a 15° rotation of one monomer around an axis of rotation; this axis passes through the two-fold dimer axis at an angle of 94.8° and at a point 2.4 Å away from the center of the dimer in the direction of the allosteric sites (see Fig. 2). There is also a translational part 2.8 Å along the axis of rotation. As a result of the rotation of both monomers relative to each other, almost all contacts between the monomers at the dimer interface are rearranged. Further local changes in the allosteric and catalytic domains after superposition are described below.

‖The direction of all movements described in this paper refers to the superposition from the T state to the R state (T-to-R transition).

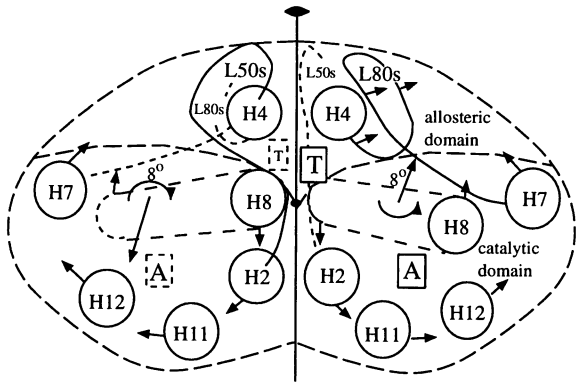

FIG. 2. Simplified scheme illustrating the movements of the main secondary structure elements from the T state to the R state. "A" marks the active site and "T" marks the allosteric site. As an alternative to two rotations by 8° of both monomers of the dimer, the transition may be described as a clockwise rotation by 15° of the left monomer around the point marked near the center of the dimer on the two-fold axis when the right monomer is held fixed.

The Allosteric Site. Tyrosine binds to YCM at the same binding site of each monomer as does tryptophan. No other binding site was found. This site thus constitutes the allosteric site of YCM activation and inhibition. The differences between R state and T state structures, as outlined above, corroborate this finding in that these changes seem to originate from the tyr/trp binding site. Since the surrounding protein residues move in different directions, it seems most sensible to superpose this region using only one of the surrounding secondary structure elements. Fig. 3 shows the allosteric binding site after superposition using residues B133–B152 of helix H8 and the 130s loop (rmsd, 0.28 Å). The effectors tyr and trp are similarly oriented in the binding site. Indeed, they show similar interactions of their carboxylate and amino groups with residues Gly-141A and Ser-142A (Table 3). However, the side chain of Arg-75A changes conformation so that it interacts with the carboxylate group of tyr but not with that of trp. The phenol ring of tyr binds at the place of the five-membered ring of the trp side chain. Its phenolic hydroxyl group interacts with the guanidinium group of Arg-76A and with the hydroxyl group of Thr-145B by hydrogen bonding. These interactions are obviously important in the formation of the T state since phenylalanine does not inhibit the enzyme. One important difference between the polar interactions of tyr and trp is that trp does not have polar contacts to residues of the allosteric domain, whereas tyr is hydrogen bonded to the side chains of Arg-75 and -76. It is also clear from Fig. 3 that the six-membered ring of trp would very closely approach several main and side-chain atoms of Ile-74A if H8 on one side and H4/H5 and the 80s loop on the other side did not move apart by about 2.7 Å.

CM from *Arabidopsis thalia*, which shares 41% sequence identity to YCM, also shows an allosteric regulation; it is activated by tryptophan and is inhibited by phenylalanine and tyrosine (22). Arg-76, Asn-139, Gly-141, and Ser-142 of YCM are conserved in the enzyme of *A. thalia*, whereas Arg-75 and Thr-145 of YCM are a glycine and a valine side chain in *A. thalia* CM, respectively. Asn-137 of YCM is missing in *A. thalia* CM.

The Active Site. After superposition of the catalytic domain based on residues 1–45, 100–213, and 231–254, further local shifts are observed of the secondary structure elements and of single residues within each catalytic domain. These shifts might affect the catalytic activity (Fig. 4). The C_α atoms of the active site residues deviate between 0.3 Å and 1.3 Å between the T and R state structures. In the T-to-R transition, movements of C_αs occur toward the active site cavity, except for Lys-168 and Glu-198. However, Glu-198 has a different side-chain confor-

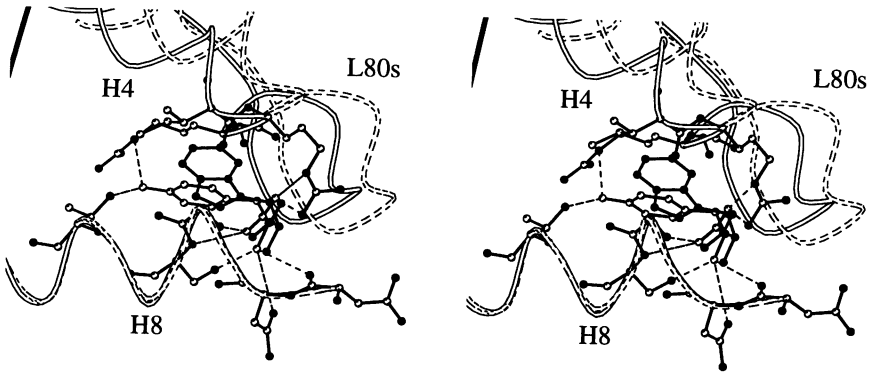

FIG. 3. Superposition of tyr and trp using residues B133–B152. Protein residues are only shown for residues Asn-138B, Asn-139B, Gly-141B, Ser-142B, Thr-145B, Ile-74A, Arg-75A, and Arg-76A of the T state structure. Polar contacts of tyr to these residues are shown as broken lines. The C_α trace of the R state structure is superimposed in broken lines to demonstrate the shift of helices H4/H5 and the 80s loop. The line in the upper left corner marks the position of the two-fold dimer axis.

mation in the R form; its carboxylate group is thereby shifted toward the active site cavity. Additional changes in side-chain conformations are observed for Arg-157 and Arg-16. The carboxylate side chain of Glu-23 moves by 5.3 Å into the active site cavity so that it forms a hydrogen bond to the guanidinium group of Arg-157 in the T state. This interaction could reduce the substrate binding affinity of Arg-157 by modulating the electrostatic field or by changing the position of the guanidinium group. Nevertheless, none of these polar active site side chains is displaced in such a way that we would be able to analyze which of the movements are primarily responsible for the different activities in the two allosteric states. Therefore, a more detailed analysis of the changes of the enzyme–substrate interactions between T and R state and its effects on catalysis requires a structural characterization of suitable enzyme–inhibitor or enzyme–substrate complexes for both states. The results reported here indicate that the 100-fold change in enzyme activity between the T and R states might be achieved by a relative movement of some of the catalytic side chains toward the active site cavity.

Local Shifts in the Catalytic Domain in Relation to the Allosteric Pathway. As outlined above, the overall allosteric T-to-R transition may be described as a 8° rotation of each of the two monomers relative to each other and a translational shift of 0.7 Å. This rotation is not followed by the 80s loop and helices H4/H5; these regions move away from the allosteric site in a direction opposite from that implied by the rotation of the catalytic domain of the same monomer. These shifts are caused by the binding of trp. Although trp binds similarly to tyr, its larger steric size pushes the C-terminal part of helices H4/H5 along with the 80s loop away from the N-terminal part of helix H8 of the other monomer. These relatively large movements can cause smaller local changes within the four-helix bundle and within the active site by forces originating from the dimer interface and from the interface between the allosteric and catalytic domains of each monomer. Rearrangements at the dimer interface result from the movement of both monomers relative to each other. One such local shift occurs in the region of residues 21–35 of helix H2, which shows a movement of about 1.7 Å toward the dimer interface. Additional shifts are observed in the regions where the 80s loop interacts with the catalytic domain of the same monomer. The C-terminal part of helix H8 is moved toward the active site, whereas the N-terminal part moves in the opposite direction (yielding a slight rotation of the long H8 helix). In the T-to-R transition, the 80s loop moves closer to helix H8 of the rotating four-helix bundle. The 80s loop interacts with the C-terminal part of helix H8, including several mainly hydrophobic contacts. The resulting rotation of helix H8, including the shift of the presumed catalytic residues Arg-157 and Lys-168 toward the active site cavity, might result from the movement of the 80s loop toward the C-terminal part of this helix, and from the interactions with the allosteric site of the other monomer at the N-terminal region of H8.

Residues of helices H11 and H12 also show significant shifts in direction toward the active site, which decrease with distance from the 220s loop connecting the two helices (Fig. 5). Both movements may be caused by the 220s loop. Although part of this loop is disordered in both crystal structures, those residues for which density is present clearly indicate that the loop moves significantly between the R and T state. In the R state, the loop continues in the same direction as helices H11 and H12 and is thereby near helices H2 and H11 of the other monomer. These interactions may shift H2 and H11 toward the active site. In the T state structure, the 220s loop points away from the catalytic domain of the other monomer. This loop probably adopts another conformation in the T state because after the 8° rotations of both monomers residues of this loop would too closely approach residues of helices H2 and H11 if it were in the same conformation as in the R state. This influence of the 220s loop on the helices H2, H11, and H12 might also explain the role of Thr-226 in the allosteric mechanism. Thr-226 is the last residue of the 220s loop next to helix H12 and it probably influences the conformation(s) of this loop. We modeled the Thr-226 side chain such that the alcohol group is hydrogen bonded to a tightly bound water molecule, which is also hydrogen bonded to the carbonyl group of Arg-224. Alternatively, in a different side-chain conformation the alcohol group might be hydrogen bonded to the carboxylate group of Glu-228. The electron density maps do not allow a distinction between these two possibilities. The T226I mutant is trapped in the R state and is not inhibited by tyr. Either of the two possible polar interactions of Thr-226 might therefore

Table 3. Selected polar contacts of ligands tryptophan and tyrosine

tyr/trp atom	Protein atom	tyr	trp* A	trp* B
N	Asn-138B O	3.8	3.3	3.3
	Asn-139B Oδ1	3.5	3.1	3.2
	Ser-142B Oγ	2.4	2.7	2.9
O	Gly-141B N	2.8	3.1	2.8
	Ser-142B N	2.8	3.0	3.0
O′	Arg-75A Nε	2.7	5.1	4.8
	Arg-75A Nη2	3.2	5.0	4.9
OH	Arg-76A Nε	3.3		
	Thr-145B Oγ1	3.1		

*The two values refer to the two independent monomers of the CM dimer in the R state crystal form.

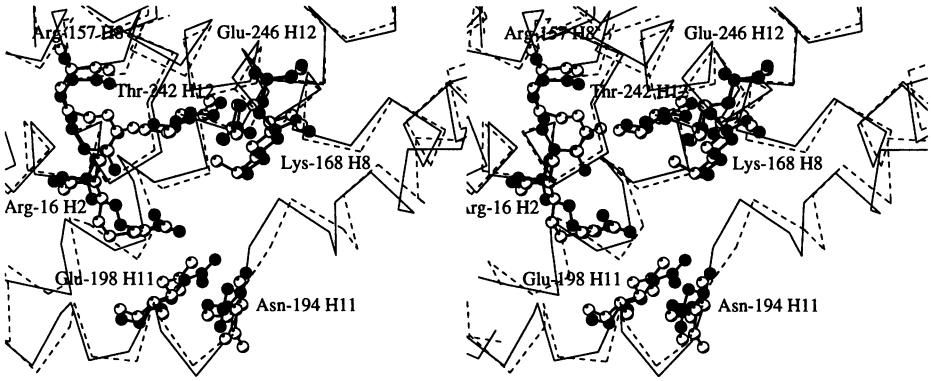

FIG. 4. Superposition of the active site regions of the A monomers of the T state (solid lines, white atoms) and the R state (broken lines, black atoms) structures after the rotation and translation. Side-chain atom positions are shown only for the presumed active site ligands. The superposition reveals further shifts that may regulate the catalytic activity within the catalytic domain.

be necessary in the formation of the T state. Unfortunately, the N-terminal part of helix H12, including Thr-226, is involved in crystal packing interactions, which might also influence the conformation of this region.

If the activation by trp is caused by an increase in the distance between residues of helix H8 and residues of helices H4/H5 and the 80s loop of the other monomer, we might assume that this distance in wild-type YCM in the absence of tyr and trp is somewhere between that found in the tyr-bound R state and the trp-bound T state. How then can tyr inhibit YCM? In other words, which interactions bring H8 and H4/H5/L80s closer together when tyr is bound compared to the wild-type enzyme? This inactivation is most probably caused by the hydrogen bonding interactions of the phenolic alcohol group as well as by the interactions of the carboxylate and amino group of tyr with residues of helix H8 and H4/H5/L80s, thereby bringing these regions closer together (Table 3, Fig. 3). In contrast, trp does not show polar interactions with H4/H5.

In summary, this structure provides a starting point for studies of mutants which test the structural basis for activity and regulation in this allosteric enzyme. The design of inhibitors on the basis of structural information in CMs, which are present only in archaebacteria, eubacteria, plants, and fungi, have the potential for development of bacteriocides, herbicides, and fungicides that inhibit an enzyme not present in humans and animals.

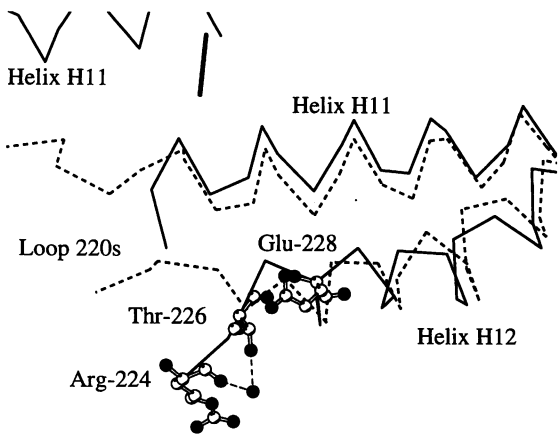

FIG. 5. Superposition of helices H11 and H12 and ordered residues of the 220s loop of the A monomers of the T-state (solid lines) and the R state (broken lines) structures after rotation and translation. Atom positions are shown for residues Arg-224, Thr-226, and Glu-228 of the T state structure and a water molecule hydrogen bonded to the main chain carbonyl group of Arg-224 and the side chain of Thr-226. Also shown is the nearby two-fold dimer axis.

Note added in proof. Summary of allosteric pathways (active site residues are in italics and the helix bundle is H2, H8, H11, and H12). Tyr brings H8 and H4/L80s together by binding to both Thr-145B and Arg-76A to favor the tighter T state, whereas trp pushes H8 and H4/L80s apart to favor the looser R state. H8 (140–171) connects the allosteric site (e.g., Gly-141 and Ser-142) to the active site (*Arg-157* and *Lys-168*) 30 Å away. H2 (14–3) includes *Arg-16* and also Glu-23 which binds to *Arg-157* in the T state only and which moves 5 Å in the T-to-R transition as H2 moves 1.7 Å. Parts of H11 (195–211) and H12 (227–215) including *Asn-194, Glu-198, Glu-246,* and *Thr-242* move toward the active site in this transition, probably aided by the 220's loop (212–226).

This work is supported by National Institutes of Health Grant GM 06920 (W.N.L.). N.S. thanks the Deutsche Forschungsgemeinschaft for financial support.

1. Weiss, U. & Edwards, J. M. (1980) *The Biosynthesis of Aromatic Amino Compounds* (Wiley, New York).
2. Braus, G. H. (1991) *Microbiol. Rev.* **55,** 349–370.
3. Sogo, S. G., Widlanski, T. S., Hoare, J. H., Grimshaw, C. E., Berchthold, G. A. & Knowles, J. R. (1984) *J. Am. Chem. Soc.* **106,** 2701–2703.
4. Copley, S. D. & Knowles, J. R. (1985) *J. Am. Chem. Soc.* **107,** 5306–5308.
5. Hilvert, D., Carpenter, S. H., Nared, K. D. & Auditor, M.-T. M. (1988) *Proc. Natl. Acad. Sci. USA* **85,** 4953–4955.
6. Jackson, D. Y., Jacobs, J. W., Sugaswara, R., Reich, S. H., Bartlett, P. A. & Schultz, P. G. (1988) *J. Am. Chem. Soc.* **119,** 4841–4842.
7. Chook, Y. M., Gray, J. V., Ke, H. & Lipscomb, W. N. (1994) *J. Mol. Biol.* **240,** 476–500.
8. Gray, J. V. & Knowles, J. R. (1994) *Biochemistry* **33,** 9953–9959.
9. Xue, Y., Lipscomb, W. N., Gray, R., Schnappauf, G. & Braus, G. (1994) *Proc. Natl. Acad. Sci. USA* **91,** 10814–10818.
10. Lee, A. Y., Karplus, P. A., Ganem, B. & Clardy, J. (1995) *J. Am. Chem. Soc.* **117,** 3627–3628.
11. Lee, A. Y., Stewart, J. D., Clardy, J. & Ganem, B. (1995) *Curr. Biol.* **2,** 196–203.
12. Xue, Y. & Lipscomb, W. N. (1995) *Proc. Natl. Acad. Sci. USA* **92,** 10595–10598.
13. Schmidheini, T., Mosch, H.-U., Evans, J. N. S. & Braus, G. (1990) *Biochemistry* **29,** 3660–3668.
14. Kabsch, W. (1988) *J. Appl. Crystallogr.* **21,** 916–924.
15. Navaza, J. (1994) *Acta Crystallogr. A* **50,** 157–163.
16. Brünger, A. T. (1992) X-PLOR Manual (Yale Univ., New Haven, CT), Version 3.1.
17. Brünger, A. T. (1992) *Nature (London)* **355,** 472–475.
18. Brünger, A. T., Krukowski, A. & Erickson, J. W. (1990) *Acta Crystallogr. A* **46,** 585–593.
19. Jones, T. A. & Kjeldgaard, M. (1994) in *From First Map to Final Model: Proceedings of the CCP4 Study Weekend*, eds. Bailey, S., Hubbard, R. & Waller, D. (Daresbury Lab., Warrington, U.K.), pp. 1–13.
20. Luzzati, V. (1952) *Acta Crystallogr. A* **5,** 801–810.
21. Kraulis, P. (1991) *J. Appl. Crystallogr.* **24,** 946–950.
22. Eberhard, J., Raesecke, H.-R., Schmid, J. & Amrhein, N. (1993) *FEBS Lett.* **334,** 233–236.